
Intrinsic and Extrinsic Organized Attention: Softmax Invariance and Network Sparsity

Oluwadamilola Fasina^{1,2}, Ruben V.C. Pohle^{2,3}, Pei-Chun Su^{1,2}, Ronald R. Coifman^{1,2,4}

¹ Department of Applied and Computational Mathematics, Yale University

² Graduate School of Arts and Sciences, Yale University

³ Medical Sciences Division, University of Oxford

⁴ Department of Mathematics, Yale University

Abstract

We examine the intrinsic (within the attention head) and extrinsic (amongst the attention heads) structure of the self-attention mechanism in transformers. Theoretical evidence for invariance of the self-attention mechanism to softmax activation is obtained by appealing to paradifferential calculus, (and is supported by computational examples), which relies on the intrinsic organization of the attention heads. Furthermore, we use an existing methodology for hierarchical organization of tensors to examine network structure by constructing hierarchal partition trees with respect to the query, key, and head axes of network 3-tensors. Such an organization is consequential since it allows one to profitably execute common signal processing tasks on a geometry where the organized network 3-tensors exhibit regularity. We exemplify this qualitatively, by visualizing the hierarchical organization of the tree comprised of attention heads and the diffusion map embeddings, and quantitatively by investigating network sparsity with the expansion coefficients of individual attention heads and the entire network with respect to the bi and tri-haar bases (respectively) on the space of queries, keys, and heads of the network. To showcase the utility of our theoretical and methodological findings, we provide computational examples using vision and language transformers. The ramifications of these findings are two-fold: (1) a subsequent step in interpretability analysis is theoretically admitted, and can be exploited empirically for downstream interpretability tasks (2) one can use the network 3-tensor organization for empirical network applications such as model pruning (by virtue of network sparsity) and network architecture comparison.¹

1 Introduction

Its widely accepted the transformer architecture [1, 2, 3, 4] transformed the fields of language and vision processing [5, 6]; however, there still exists a measurable gap between its theoretical underpinnings, and incidentally, the interpretability of the transformer architecture [7, 8, 9, 10, 11]. Examples of efforts to close such gaps are [12, 13] who discuss theoretical learning capabilities of transformers and [14] and [15] who discuss the explainability and internal structure of transformers. Studies of this flavor have aided in closing the gap between theory, empirical findings, and explainability of the fabric of transformer architectures, and we aim to contribute to this by approaching these issues through the conceptual and mathematical lens of tensor organization.

The self-attention mechanism is used in virtually every transformer network and has been proven to be crucial, in fact, necessary for transformers to learn effectively [16, 17]. Indeed, its ability to

¹Code is available at <https://github.com/obfasina/OrganizedAttention/>

capture pairwise relationships amongst input tokens allows it to learn the inherent structure of the data in consideration. We, like others, conjecture that exploitation of information carried by the attention heads brings light to salient network structure. We constrain our focus to two types of analysis: intrinsic and extrinsic self-attention organization. We show theoretically - and supplement with computational examples - that if one produces an intrinsic organization of the attention head to have some regularity, the self-attention mechanism is invariant to the softmax function. Secondly, we describe an algorithm that admits an extrinsic organization of the attention heads; that is, an organization among all the heads in the network which allows us to probe the network structure, and consequently, carry out signal processing tasks economically.

2 Paraproduct Decompositions and Tensor Organization

We rely on two principal analytical tools for imputing salient intrinsic and extrinsic organization of attention heads: paraproduct decompositions and tensor organization. Paraproduct decompositions, or so called paradifferential calculus, was initiated by [18] and had a sizable impact in diverse subdisciplines of pure and applied mathematics such as operator theory, fourier analysis, and PDE. [19, 20, 21]. Informally, paradifferential calculus is concerned with decomposing operators into their low and high frequency constituents. Recently, Bony's work was extended by [22], facilitating similar decompositions for smooth nonlinear transformations of tensors with mixed-holder regularity.

The second tool is the questionnaire method originally described in [23, 24, 25] for organizing tensors. The questionnaire method relies on a key insight: understanding coordinates of each axis of a tensor as graphs to be organized with respect to the geometry of the other graphs induced by the axes of a tensor leads to a coherent tensor organization. Crucially, such a tensor organization allows for the data to be smooth with respect to the underlying geometry (the tensor product of graphs defined with respect to each axis in this setting), permitting one to consider further tensor inference questions such as sparsity and approximation. Indeed, in [26, 27, 28] the questionnaire method was utilized for inferring the spatio-temporal structure of neuronal data, enabling dynamic equation discovery governing chemical and bioengineering processes, and, general PDE discovery, respectively. As these two instruments are key to our empirical findings, we expound on their formulations in the subsequent subsections.

2.1 Tensor Paraproducts

We retain the notation used in [22] to describe tensor paraproduct decompositions in our setting. First we begin with a few definitions describing Holder and mixed Holder regularity, a key regularity assumption required for the decomposition to hold.

Definition 1. A function, $f : x \in [0, 1] \rightarrow \mathbb{R}$ is α -Holder with respect to the distance metric $d(x, y)$ satisfies the following the condition:

$$\frac{|f(x) - f(y)|}{|d(x, y)|^\alpha} \leq C \quad \forall x, y \in \mathbb{R} \quad (1)$$

where $C, \alpha > 0$. We denote the set comprised of such functions as $\Lambda^\alpha([0, 1])$

Definition 2. A function $f : (x, x') \in [0, 1]^2 \rightarrow \mathbb{R}$ which is mixed α -Holder with respect to the distance metrics $d(x, y), d'(x', y')$ satisfies the following conditions.

$$\begin{aligned} \frac{|f(x, x') - f(y, x')|}{|d(x, y)|^\alpha} &\leq C, \quad \frac{|f(x, x') - f(x, y')|}{|d'(x', y')|^\alpha} \leq C, \\ \frac{|f(y, y') - f(x, y') - f(y, x') + f(x, x')|}{|d(x, y)|^\alpha |d'(x', y')|^\alpha} &\leq C \quad \forall x, x' \in [0, 1]^2, \end{aligned} \quad (2)$$

with $C, \alpha > 0$. We denote this space as tensor- $\Lambda^\alpha([0, 1]^2)$, but we refer to the space of such functions as $\Lambda^\alpha([0, 1]^2)$ in the rest of the paper, for brevity.

As described in [29, 30], Holder regularity and wavelets are intimately related as wavelet coefficients can be used to characterize Holder regularity and vice versa. Wavelets have a storied theoretical [31] and applied [32, 33] history; this is due in no small part to their ease in computability (for certain wavelet families) and locality of in frequency and time. Here we consider Haar wavelet system though the tensor decomposition holds for any family of wavelets.

Definition 3. (*Wavelets and Tensor Wavelets for Haar System*) For $j, k \in \mathbb{N}$, the interval I_k^j in direction x is defined to be the set of points contained in the k th interval at scale j .

$$I_k^j = \{x : x \in (2^{-j}k, 2^{-j}(k+1)]\} \quad (3)$$

We can then construct the scaling, $\phi_k^j(x)$, and wavelet functions, $\psi_k^j(x)$, supported on the k th interval at scale j :

$$\phi_k^j(x) \begin{cases} 1 & x \in I_k^j \\ 0 & x \notin I_k^j \end{cases} \quad (4)$$

$$\psi_k^j(x) \begin{cases} 1 & x \in I_{k+}^j \\ -1 & x \in I_{k-}^j \end{cases} \quad (5)$$

where $I_{k-}^j = \{x : x \in (\inf_I(I_k^j), \inf_I(I_k^j) + \frac{(\inf_I(I_k^j) + \sup_I(I_k^j))}{2})\}$ and $I_{k+}^j = \{x : x \in (\frac{(\inf_I(I_k^j) + \sup_I(I_k^j))}{2}, \sup_I(I_k^j)]\}$. The scaling and wavelet functions in the x' direction are defined the same modulo a change of notation:

$$I_k^{j'} = \{x' : x' \in (2^{-j'}k, 2^{-j'}(k+1)]\} \quad (6)$$

$$\phi_k^{j'}(x') \begin{cases} 1 & x' \in I_k^{j'} \\ 0 & x' \notin I_k^{j'} \end{cases} \quad (7)$$

$$\psi_k^{j'}(x') \begin{cases} 1 & x' \in I_{k+}^{j'} \\ -1 & x' \in I_{k-}^{j'} \end{cases} \quad (8)$$

where $I_{k+}^{j'}$, $I_{k-}^{j'}$ are defined in the same sense as I_{k+}^j , I_{k-}^j . Finally we define the tensor scaling and tensor wavelet functions for $x, x' \in [0, 1] \times [0, 1]$

$$\phi_{k,k'}^{j,j'}(x, x') = \phi_k^j(x) \otimes \phi_{k'}^{j'}(x') \quad (9)$$

$$\psi_{k,k'}^{j,j'}(x, x') = \psi_k^j(x) \otimes \psi_{k'}^{j'}(x') \quad (10)$$

Remark 1. The wavelet and tensor wavelet functions are defined for the sake of exposition but the decomposition is formulated and can be explicitly computed only with the tensor scaling function.

Theorem 1. Suppose $A \in C^2$, $f \in \Lambda^\alpha([0, 1]^2)$, $0 < \alpha < \frac{1}{2}$, then we obtain the following discrete multiscale tensor decomposition of $A(f)$:

$$P^j P^{j'}(f) = \sum_{k=1}^{2^j} \sum_{k'=1}^{2^{j'}} P_k^j P_{k'}^{j'}(f) = \sum_{k=1}^{2^j} \sum_{k'=1}^{2^{j'}} \left(\frac{1}{|R_{k,k'}^{j,j'}|} \int_{R_{k,k'}^{j,j'}} f(y, y') \phi_{k,k'}^{j,j'}(y, y') dy dy' \right) \chi_{R_{k,k'}^{j,j'}}(x, x') \quad (11)$$

$$\begin{aligned}
A(f) &= \sum_{j'=0}^{N'} \sum_{j=0}^N A'(P^j P'^{j'}(f)) [P^{j+1} P'^{j'+1}(f) - P^j P'^{j'+1}(f) - P^{j+1} P'^{j'}(f) + P^j P'^{j'}(f)] \\
&+ A''(P^j P'^{j'}(f)) [P^{j+1} P'^{j'}(f) - P^j P'^{j'}(f)] [P^j P'^{j'+1}(f) - P^j P'^{j'}(f)] + \Delta_{N,N'}(A, f) \quad (12)
\end{aligned}$$

$$A(f) = \tilde{A}(f) + \Delta_{N,N'}(A, f) \quad (13)$$

$$\Delta_{N,N'}(A, f) = A(f) - \tilde{A}(f) \in \Lambda^{2\alpha}([0, 1]^2) \quad (14)$$

where $\Delta_{N,N'}(A, f)$ is the residual between $A(f)$ and $\tilde{A}(f)$ up to scales N, N' . $P^j P'^{j'}$ is a convolution operators acting on f with the tensor product of the scaling functions, $\phi_{k,k'}^{j,j'}(x, x')$, at scales j, j' as its kernel. $R_{k,k'}^{j,j'} = I_k^j \times I_{k'}^{j'}$ is a dyadic rectangle constructed from taking the product of dyadic intervals $I_k^j, I_{k'}^{j'}$ at scales j, j' such that $|R_{k,k'}^{j,j'}| = 2^{-(j+j')}$

2.2 Tensor Organization

2.3 Questionnaire Algorithm

The questionnaire algorithm organizes tensors in a multiscale sense by leveraging the hierarchal nature of partition trees. Informally, partition trees are a type of directed graph comprised of nodes with directed edges from parents to children. They can be binary where each parent has two children, or arbitrary - where no restriction is placed on the number of children a parent can have. In our setting, the nodes of the partition trees contain indices of a tensor axis (distinct from the sample associated with the index). As each axis has its own partition tree, in this situation we have three partition trees: a distinct tree for the row, column, and channel axes. We describe mathematically and algorithmically the construction of such trees in the same sense as [26, 25] in the context of transformer networks.

Let $\mathcal{H} = \{1, 2, \dots, n_H\}, \mathcal{Q} = \{1, 2, \dots, n_Q\}, \mathcal{K} = \{1, 2, \dots, n_K\}$, denote the set of indices for the head, query, and key axes. Define $\mathcal{T}_H, \mathcal{T}_Q, \mathcal{T}_K$, to be the partition trees defined on $\mathcal{H}, \mathcal{Q}, \mathcal{K}$, respectively which contain the nodes of the tree. Let $\mathcal{Q}_k^l \subset \mathcal{Q}$ be the k th node at level l in the tree \mathcal{T}_Q which contains a subset of the query indices. Analogously, we define $\mathcal{H}_k^l, \mathcal{K}_k^l$ - nodes at level l and location k in a tree. We use a type of EMD - proved to be equivalent to traditional formulations of EMD in [34] and used in [25] - which computes affinities between 2D matrices based on where the coordinates of the matrix lie in the cartesian product between the nodes of the trees defined on the set of indices of each axis. Suppose $\mathbf{X} \in \mathbb{R}^{|\mathcal{Q}| \times |\mathcal{K}| \times |\mathcal{H}|}$ is the network 3-tensor we wish to process. Let $\mathbf{A}_p = \mathbf{X}[p, :, :], \mathbf{A}_j = \mathbf{X}[j, :, :]$. Then we define the EMD as the following:

$$\text{EMD}_{\mathcal{T}_Q \times \mathcal{T}_K}(\mathbf{A}_p, \mathbf{A}_j) = \sum_{\mathcal{Q}_k^l \in \mathcal{T}_Q, \mathcal{K}_k^l \in \mathcal{T}_K} m(\mathbf{A}_p - \mathbf{A}_j, \mathcal{Q}_k^l \times \mathcal{K}_k^l) w(\mathcal{Q}_k^l \times \mathcal{K}_k^l) \quad (15)$$

$$m(\mathbf{A}_p, \mathcal{Q}_k^l \times \mathcal{K}_k^l) = \frac{1}{|\mathcal{Q}_k^l| |\mathcal{K}_k^l|} \sum_{(q,k) \in \mathcal{Q}_k^l \times \mathcal{K}_k^l} \mathbf{A}_p[q, k], w(\mathcal{Q}_k^l \times \mathcal{K}_k^l) > 0 \quad (16)$$

where $w(\mathcal{Q}_k^l \times \mathcal{K}_k^l) > 0$ is a weight value depending on the level and size of the nodes in the trees and (q, k) are the query and key indices contained in the cartesian product of a particular set of nodes in the tree. Of course, the EMD with respect to the other axes are identical modulo a permutation of the partition trees incorporated into the computation. We summarize the questionnaire algorithm below:

Algorithm 1 3D Questionnaire

1: **procedure** BOTTOM UP FLEXIBLE TREE(Ψ)
Require: $\Psi = \{\lambda_i \Psi_i(x)\}_{i=1}^n$, an eigendecomposition of the Markov matrix
Ensure: $\mathcal{T} = \{1, 2, \dots, n(\mathcal{T})\}$ where $n(\mathcal{T})$ is the number of nodes in partition tree
2: **end procedure**
3: **procedure** INITIALIZE QUERY, KEY PARTITION TREES(\mathbf{X})
Require: $\mathbf{X} \in \mathbb{R}^{|\mathcal{Q}| \times |\mathcal{K}| \times |\mathcal{H}|}$
Ensure: $\mathcal{T}_Q^i, \mathcal{T}_K^i$
4: $\mathbf{X}_Q \in \mathbb{R}^{|\mathcal{Q}| \times |\mathcal{K}| \times |\mathcal{H}|}$
5: $\mathbf{G}_Q[i, j] \leftarrow \frac{\langle \mathbf{x}_Q^T(:, i), \mathbf{x}_Q^T(:, j) \rangle}{\|\mathbf{x}_Q^T(:, i)\| \|\mathbf{x}_Q^T(:, j)\|} \forall i, j \in \{1, 2, \dots, |\mathcal{Q}|\}$
6: $\mathbf{D}[i, j] \leftarrow \sum_m \mathbf{G}_Q[i, m]$ for $i = j$, $\mathbf{D}[i, j] \leftarrow 0$ for $i \neq j$
7: $\mathbf{M}_Q \leftarrow \mathbf{D}^{-\frac{1}{2}} \mathbf{D}^{-\frac{1}{2}} \mathbf{G}_Q \mathbf{D}^{-\frac{1}{2}} \mathbf{D}^{\frac{1}{2}}$, $\phi : \mathbf{M}_Q \rightarrow \{\lambda_i \psi_i^Q(x)\}_{i=1}^n = \Psi_Q$
8: Repeat steps 4 to 7 for $\mathbf{X}_K \in \mathbb{R}^{|\mathcal{K}| \times |\mathcal{Q}| \times |\mathcal{H}|}$ to obtain Ψ_K
9: $\mathcal{T}_Q^i \leftarrow$ BOTTOM UP FLEXIBLE TREE(Ψ_Q), $\mathcal{T}_K^i \leftarrow$ BOTTOM UP FLEXIBLE TREE(Ψ_K)
10: **return** $\mathcal{T}_Q^i, \mathcal{T}_K^i$
11: **end procedure**
12: **procedure** TENSOR ORGANIZATION($\mathcal{T}_Q^i, \mathcal{T}_K^i$)
Require: $\mathcal{T}_Q^i, \mathcal{T}_K^i, \mathbf{X} \in \mathbb{R}^{|\mathcal{Q}| \times |\mathcal{K}| \times |\mathcal{H}|}$
Ensure: $\mathcal{T}_H^o, \mathcal{T}_Q^o, \mathcal{T}_K^o, \mathbf{G}_H, \mathbf{G}_K, \mathbf{G}_Q$
13: $\mathcal{T}_Q^i, \mathcal{T}_K^i \leftarrow$ INITIALIZE QUERY, KEY, PARTITION TREES(\mathbf{X})
14: **for** $m = 1 \dots N$ **do**
15: $\mathbf{A}_p \leftarrow \mathbf{X}[:, :, p]$, $\mathbf{A}_j \leftarrow \mathbf{X}[:, :, j]$, $\text{EMD}_{\mathcal{T}_Q^i \times \mathcal{T}_K^i}[\mathbf{A}_p, \mathbf{A}_j] \forall j, p \in \mathcal{H}$
16: $\mathbf{E}_H \leftarrow \text{EMD}_{\mathcal{T}_Q^i \times \mathcal{T}_K^i}$, $\mathbf{G}_H = e^{-\frac{\mathbf{E}_H}{\epsilon}}$, $\epsilon = \text{median}(\mathbf{E}_H)$, $\phi : \mathbf{G}_H \rightarrow \mathbf{M}_H \rightarrow \{\lambda_i \psi_i(x)\}$
17: $\mathcal{T}_H \leftarrow$ BOTTOM UP FLEXIBLE TREE(Ψ_H)
18: Repeat steps 15-17 using key and head partition trees to generate query partition tree
19: Repeat steps 15-17 using query and head partition trees to generate key partition tree
20: **end for**
21: **return** $\mathcal{T}_H^o, \mathcal{T}_Q^o, \mathcal{T}_K^o, \mathbf{G}_H, \mathbf{G}_K, \mathbf{G}_Q$
22: **end procedure**

For further algorithmic details we refer the reader to [25], for more mathematical details, we refer the reader to [24], and for a different but similar exposition in 3D, [26]. The questionnaire algorithm outputs the final affinities and partition trees along each axis which are useful for downstream analysis.

2.4 Tri-Haar Basis and Sparsity

Each of the nodes contained in the output trees, $\mathcal{T}_H^o, \mathcal{T}_Q^o, \mathcal{T}_K^o$, from 2.3 contain the query, key, and head indices in each of the nodes. Consequentially, one has $f : \mathcal{T}_H^o \times \mathcal{T}_Q^o \times \mathcal{T}_K^o \rightarrow \mathbb{R} \in \mathbf{X}, \mathbf{X} \in \mathbb{R}^{|\mathcal{Q}| \times |\mathcal{K}| \times |\mathcal{H}|}$, meaning functions supported on the new geometry obtained from the questionnaire organization are just the network 3-tensor elements. It follows that construction of a suitable basis to compress f is natural and was first described in [29, 23]. We provide a brief description of a tri-haar basis on the obtained geometry following the notation of [29, 23].

Define $\psi_{l_0, k_0, j_0}^{\mathcal{H}}(x), \psi_{l_1, k_1, j_1}^{\mathcal{Q}}(y), \psi_{l_2, k_2, j_2}^{\mathcal{K}}(z)$ to be the Haar wavelets associated with the nodes $\mathcal{H}_k^l \subset \mathcal{H}, \mathcal{Q}_k^l \subset \mathcal{Q}, \mathcal{K}_k^l \subset \mathcal{K}$ which contain subsets of head, query, and key indices, at node k and level l in the tree, where j is the wavelet function associated with a particular node. Note $l_0 = 0_0, 0_1, \dots, |n(l_0)|$ where $n(l_0)$ is the number of levels in the partition tree defined on the space of heads. The superscripts k_0, j_0 for the node location and the number of associated wavelet functions are indexed similarly, and a similar notation holds for $\{l_1, k_1, j_1, l_2, k_2, j_2\}$, the superscripts for the query and key trees. Then one defines a tri-haar basis $\psi_{l_0, k_0, j_0}^{\mathcal{H}}(x) \otimes \psi_{l_1, k_1, j_1}^{\mathcal{Q}}(y) \otimes \psi_{l_2, k_2, j_2}^{\mathcal{K}}(z)$ and its associated expansion coefficients: $\bigcup_{i=0}^2 \alpha_{\{l_i, k_i, j_i\}} = \langle f(x, y, z) (\psi_{l_0, k_0, j_0}^{\mathcal{H}}(x) \otimes \psi_{l_1, k_1, j_1}^{\mathcal{Q}}(y) \otimes \psi_{l_2, k_2, j_2}^{\mathcal{K}}(z)) \rangle$. As in the Euclidean setting, such expansion coefficients can be used to measure function smoothness via the l_p entropy of the expansion coefficients as described in [23]. Of note,

one can define 2D tensor bases with respect to the different basis vectors; in fact, the tensor basis comprised of the query and key bases will be a central object in our analyses.

3 Softmax Invariance and Sparsity

We probe the intrinsic and extrinsic structure of the self-attention mechanism of two well-known transformer language and vision networks, respectively: Transformer-XL [35] and ViT B16 [36]. For both networks, we provide numerical experiments to support our theoretical finding that self-attention is invariant to softmax activation under appropriate assumptions in section 4.1. We then use the questionnaire algorithm described in 2.3 to organize the attention heads for both networks, permitting downstream network analysis. First, qualitative results of network organization are provided by a visualization of the attention heads in both networks using the diffusion maps [37] algorithm, along with the resulting partition tree and adjacency matrix between the attention heads. Subsequently, we compute the expansion coefficients with respect to the query-key tensor basis and furthermore the l_1 entropy of each attention head of the networks to understand the network sparsity.

3.1 Softmax Invariance

Theorem 2. *Let $f \in \mathbb{R}^{N \times N}$ be an attention head in a network and $\tilde{f} \in \mathbb{R}^{N \times N} \subset \Lambda^\alpha([0, 1]^2)$ be a mixed α -Holder approximation of f . Suppose $A_k(\tilde{f}_i) = \frac{e^{\tilde{f}_{i,k}}}{\sum_j e^{\tilde{f}_{i,j}}}$, where k, j are the column indices while i is a row index such that $A_k(\tilde{f}_i)$ operates pointwise on the i th row and k th column of \tilde{f} (i.e. the softmax activation function applied to \tilde{f}). Then the softmax activation on a mixed α -Holder attention head can be decomposed into:*

$$A(\tilde{f}) = A'(P^j P^{j'}(f))[P^{j+1} P^{j'+1}(f) - P^j P^{j'+1}(f) - P^{j+1} P^{j'}(f) + P^j P^{j'}(f)] \\ + A''(P^j P^{j'}(f))[P^{j+1} P^{j'}(f) - P^j P^{j'}(f)][P^j P^{j'+1}(f) - P^j P^{j'}(f)] + \Delta_{N,N'}(A, f) \quad (17)$$

Proof. This is proved directly by appealing to [22]. □

Corollary 1. *If we assume that for a network $T : \{t_i\}_{i=1}^n \rightarrow \hat{v}_m$, $L(v, \hat{v}_m) \rightarrow 0, \forall \hat{v}_m \in \mathcal{X}$, as $|[P^{j+1} P^{j'+1}(f) - P^j P^{j'+1}(f) - P^{j+1} P^{j'}(f) + P^j P^{j'}(f)]| \rightarrow \infty$ holds, then the softmax activation on a mixed α -Holder attention head can be decomposed into:*

$$A(\tilde{f}) = [P^{j+1} P^{j'+1}(f) - P^j P^{j'+1}(f) - P^{j+1} P^{j'}(f) + P^j P^{j'}(f)] \\ + [P^{j+1} P^{j'}(f) - P^j P^{j'}(f)][P^j P^{j'+1}(f) - P^j P^{j'}(f)] + \Delta_{N,N'}(A, f) \quad (18)$$

where L is a loss function, $\{t_i\}_{i=1}^n$ is a set of tokens input to the model, \hat{v}_m is a prediction from T , v is a ground truth, and \mathcal{X} is a set containing possible predictions of T and the ground truth solution, and $P^j P^{j'}(f)$ is the averaging operator defined in section 3.

Proof. See Appendix □

3.1.1 Network Descriptions

The transformer-xl (TXL) model is comprised of 16 layers, each with a multi-head attention mechanism consisting of 8 heads. We train transformer-xl on the WikiText-103 [38] dataset. Following training, we evaluate the network and 10 batches where each batch is comprised of 256 tokens. We then extract all the attention matrices for all 10 batches for downstream analysis. The ViT B16 model is comprised of 12 layers each with a multi-head attention mechanism comprised of 12 heads. The ViT model is trained on the CIFAR10 [39] dataset. Following training of the ViT model, we evaluate the network on 10 batches, where each batch is comprised of 197 tokens. Again, all the attention matrices for the 10 batches are used for downstream analysis. See the appendix for further experimental details.

3.1.2 Softmax Invariance Computational Experiments

Nomenclature We refer to a batch as a collection of tokens contained in a fixed context length. This terminology is used since we consider each token to be a sample.

For both the TXL and VIT models we considered 10 randomly selected batches of test data, which are projected onto the query and key matrices associated with each network, during inference. An attention matrix, \mathbf{A} , is constructed by projecting the data, \mathbf{X} onto the query and key weight matrices, $\mathbf{W}_Q, \mathbf{W}_K$: $\mathbf{A} = \text{softmax}(\frac{\mathbf{X}\mathbf{W}_Q\mathbf{W}_K^T}{\sqrt{D}})$ where D is the number of tokens in each batch. The TXL network is comprised of 128 attention heads while the VIT network is comprised of 144. We can define the sets of attention matrices for each of the networks as:

$$\mathcal{X}_{\text{TXL}} = \{\{\mathbf{A}_1^{(m)}\}_{m=1}^{128}, \dots, \{\mathbf{A}_{10}^{(m)}\}_{m=1}^{128}\} \quad (19)$$

$$\mathcal{X}_{\text{VIT}} = \{\{\mathbf{A}_1^{(m)}\}_{m=1}^{144}, \dots, \{\mathbf{A}_{10}^{(m)}\}_{m=1}^{144}\} \quad (20)$$

where $\mathbf{A}_i^{(m)}$ is the attention head associated with the m th weight matrix for the i th batch. For the TXL network, $\mathbf{X} \in \mathbb{R}^{256 \times d}$ where d is the model dimension while for the VIT network, $\mathbf{X} \in \mathbb{R}^{197 \times d}$ where d is the model dimension for the VIT network. 256 and 197 correspond to the number of tokens in the TXL and VIT networks, respectively.

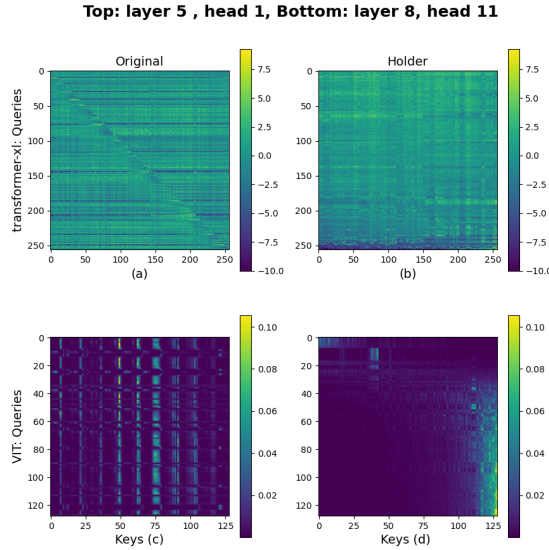


Figure 1: Organization of two randomly selected attention heads (top is from TXL, bottom is from VIT) to have mixed α -Holder regularity (a) original TXL attention head (b) organization of TXL attention head (c) original VIT attention head (d) organization of VIT attention head to have mixed α -Holder regularity

We randomly selected one of the 10 batches from both the WikiText-103 and CIFAR-10 datasets. On the left column is a visualization of the extracted attention heads for the TXL (top) and VIT (bottom) networks. On the right are the corresponding mixed α -Holder organizations of the matrix. We remark that the attention head for the VIT network was cropped to have a dimension (128) on each axis, as having dimensions which are a power 2 are a necessary requirement for the implementation. The organization of a matrix to be mixed α -holder is simply a 2D version of the 3D questionnaire

algorithm described in the main text; further details can be found in the references associated with the 3D questionnaire algorithm. This organization is essential, as the decomposition theorem in the main text only holds for smooth nonlinear transformation of functions with mixed α -Holder regularity. One can qualitatively see the smoothness in the right column in contrast to the left for both the TXL and VIT networks.

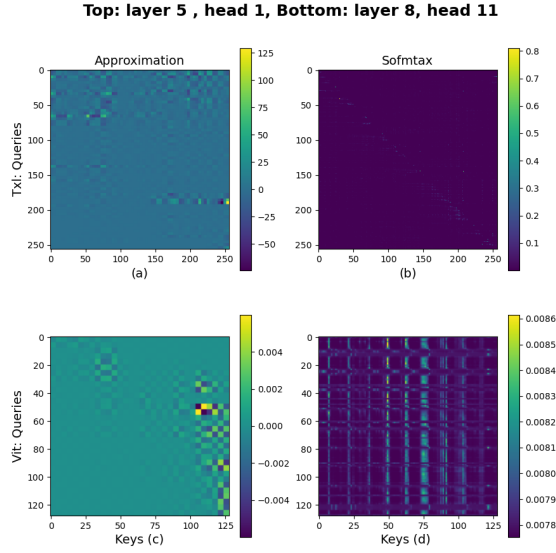


Figure 2: Paraproduct decomposition and softmax attention mechanism applied to both attention heads in 1. (a) approximation of TXL attention head with the paraproduct decomposition (b) Softmax of TXL attention head (c) approximation of VIT attention head with the paraproduct decomposition (d) softmax of VIT attention head

We implement the decomposition theorem on the same attention heads considered in Figure 1. The left column is the approximation, the right column is the softmax activation function applied to the mixed α -Holder attention heads. For the TXL attention, its readily seen the softmax activation function oversquashes certain coordiantes in the attention head, while the approximation preserves some of the structure. A similar phenomenon is seen for the VIT attention head, though less pronounced.

3.2 Network Sparsity

We organized network 3-tensors of concatenated attention heads for both the TXL and VIT networks such that one can qualitatively and quantitatively assess the organization among all the heads in the network. For each batch comprised of 256 and 197 tokens for the WikiText-103 and CIFAR-10 datasets respectively, we deploy the questionnaire algorithm to organize the corresponding network 3-tensors: $\{\mathbf{A}_i^{(m)}\}_{m=1}^{128} \in \mathcal{X}_{\text{TXL}}, \{\mathbf{A}_i^{(m)}\}_{m=1}^{144} \in \mathcal{X}_{\text{VIT}}$.

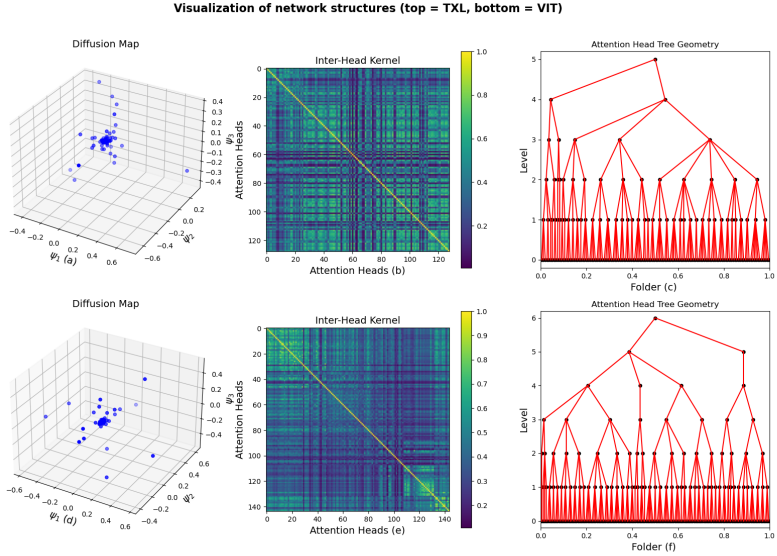


Figure 3: Visualization of resulting network structure from diffusion maps algorithm. (a) Diffusion map embedding of TXL attention heads (b) Adjacency matrix of TXL attention heads (c) flexible tree comprised of TXL attention heads (d) Diffusion map embedding of VIT attention heads (e) Adjacency matrix of VIT attention heads (f) flexible tree comprised of VIT attention heads

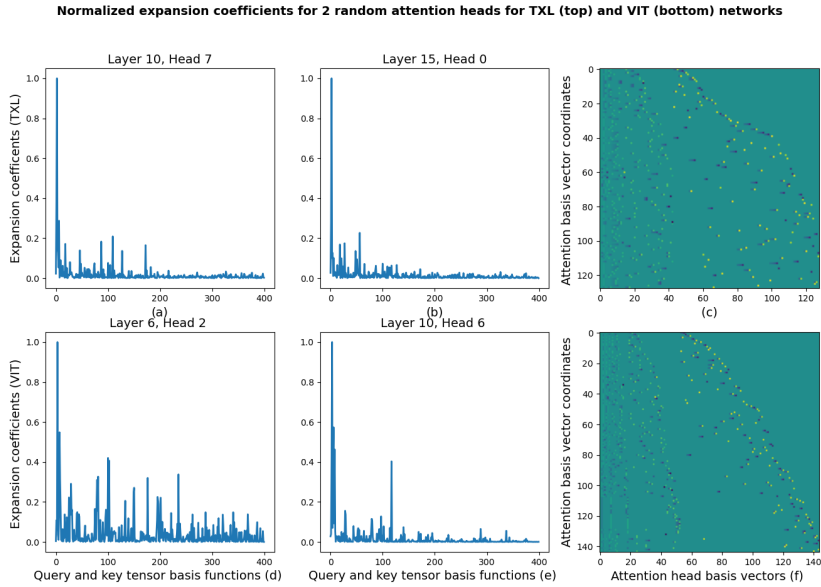


Figure 4: Expansion coefficients of two random attention heads from both the TXL (top) and VIT (bottom) networks obtained from projecting an attention head into query-key tensor basis. For each network, plots of expansion coefficients are sorted in descending order from largest to smallest query-key tensor basis support size (a) Expansion coefficients for head 7 in layer 10 of the TXL network (b) Expansion coefficients for head 0, layer 15 in the TXL network (c) Haar basis vectors for the TXL attention head space (d) Expansion coefficients for head 7 in layer 10 of the VIT network (e) Expansion coefficients for head 6 in layer 10 of the VIT network (f) Haar basis vectors for the VIT attention head space

The questionnaire algorithm outputs (a) a partition tree on the space of heads, where each tree contains a folder comprised of the head indices, (b) an affinity matrix comprised of pair-wise similarities between each of the attention heads in the network. We also subsequently built (c) a diffusion map using the affinity matrix of pair-wise relations between attention-heads. The top and bottom rows of Figure 3 are used to qualitatively assess the organization of the network for one batch of data for the TXL and VIT networks, respectively. The diffusion map on the TXL network exhibits some continuous structure, while the VIT network is more clustered and contains some outliers.

In Figure 4 we visualized the decay of the expansion coefficients by projecting each attention head on the the bi-haar basis of queries and keys. Let $\bigcup_{i=0}^1 \beta_{\{l_i, k_i, j_i\}} = \langle f(x, y, \cdot), \psi_{l_1, k_1, j_1}^Q(x) \otimes \psi_{l_2, k_2, j_2}^H(y) \rangle$ be an expansion coefficient obtained from projecting into the bi-haar basis of queries and keys. The indices (l, k, j) denote the level, location, and index of a basis function of a tree, respectively. the subscripts of 0 and 1 are used to denote the basis functions for the query and key binary trees, respectively.

The left and middle columns are plots of the expansion coefficients (sorted in descending order by the query and key bi-haar basis support size) obtained by projecting two randomly selected heads into the query and key bi-haar basis. We consider the 400 tensor basis vectors with largest support size. The right column is a visualization of the basis vectors defined for the tree associated with the attention heads. The top and bottom rows are for the TXL and VIT networks, respectively. The distribution of expansion coefficients is similar for all attention heads.

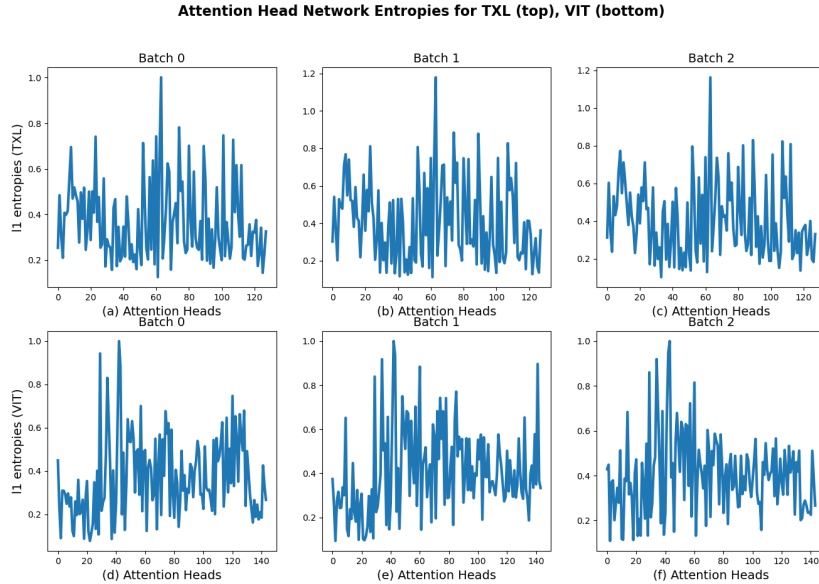


Figure 5: Network l_1 entropies, obtained by projecting a function into tensor product of query and key bases. (a) - (c) Network entropy from projecting into query-key tensor basis (d) - (f) Network entropy from projecting into query-key tensor basis

For each network we consider 3 batches each comprised of 256 and 197 tokens for the TXL and VIT, respectively. We compute the l_1 entropy of the expansion coefficients for each of the heads in the network by summing over the magnitude of the expansion coefficients associated with the top 400 basis vectors:

$$\|\beta\|_{l_1} = \sum_{\text{supp}(\psi^Q(x) \otimes \psi^H(y)) > \epsilon} \left| \bigcup_{i=0}^1 \beta_{\{l_i, k_i, j_i\}} \right| \quad (21)$$

where ϵ is a threshold for the 400 tensor basis vectors with largest support size, and β is a vector containing the 400 expansion coefficients. Note that each batch of data corresponds to a different collection of network attention heads since projection of this batch onto the query and key weight matrices results in a different attention head. Qualitatively, we can see a consistent spread of network entropies for both the TXL (top) and VIT (bottom) networks across the batches of data. An attention head with high l_1 entropy with respect to the query-key tensor basis relative to the rest of the network heads indicates that attention head is involved in a lot of processing as its attention head is picking up the sharp transitions within the attention head. The converse can be said for low l_1 entropy relative to the rest of the network. This qualitative finding (a) validates our organization method in the sense that a similar l_1 entropy network spread is seen for different batches within a network (b) suggests this technique could be used for model pruning; the head with low l_1 entropy do little processing and could be discarded.

4 Conclusion and Limitations

We demonstrated how penetrating the intrinsic and extrinsic structure leads to useful theoretical and empirical insights. We rely on the questionnaire algorithm to intrinsically and extrinsically organize the attention heads. The intrinsic organization permits the attention head to have Holder regularity, allowing us to connect this result to existing theory, revealing the self-attention mechanism is invariant to the softmax activation function. The extrinsic organization allows one to qualitatively and quantitatively understand network structure. Qualitative inference constitutes construction of the diffusion maps algorithm on the affinity matrix between network heads as well as the hierarchical tree geometry of the attention heads, which are both output from the questionnaire algorithm. Quantitative inference consists of computing the entropy of the attention heads with respect to the bi-haar basis and the entropy of the network with respect to the tri-haar basis (see appendix).

Our main theoretical finding of softmax invariance has some restrictive assumptions. First, it requires the attention head to be organized to have mixed α -Holder regularity. While this can be achieved using the questionnaire algorithm, the mixed α -Holder attention head loses its original intrinsic structure since the matrix elements are permuted based on the location of the row and column indices in their respective binary trees. Incidentally, the mixed α -Holder attention head (as organized by the questionnaire algorithm) and the original attention head are only equivalent up to large constants. A minor empirical restriction is implementation of the computational examples of the theorem requires the attention head to be a power of 2, which can force one to crop the attention matrix for further downstream analysis (e.g. VIT attention heads were cropped from 197 to 128). Additionally, the questionnaire algorithm can be sensitive to the algorithm parameters such as the affinity initialization and the weight function used during the iterative EMD process. Nevertheless, we envision and hope the theoretical and methodological contributions in this paper can be deployed for model pruning or general network interpretability tasks.

References

- [1] Ashish Vaswani, Noam Shazeer, Niki Parmar, Jakob Uszkoreit, Llion Jones, Aidan N Gomez, Łukasz Kaiser, and Illia Polosukhin. Attention is all you need. *Advances in neural information processing systems*, 30, 2017.
- [2] Yi Tay, Mostafa Dehghani, Dara Bahri, and Donald Metzler. Efficient transformers: A survey. *ACM Computing Surveys*, 55(6):1–28, 2022.
- [3] Salman Khan, Muzammal Naseer, Munawar Hayat, Syed Waqas Zamir, Fahad Shahbaz Khan, and Mubarak Shah. Transformers in vision: A survey. *ACM computing surveys (CSUR)*, 54(10s):1–41, 2022.
- [4] Tianyang Lin, Yuxin Wang, Xiangyang Liu, and Xipeng Qiu. A survey of transformers. *AI open*, 3:111–132, 2022.
- [5] Prakash M Nadkarni, Lucila Ohno-Machado, and Wendy W Chapman. Natural language processing: an introduction. *Journal of the American Medical Informatics Association*, 18(5):544–551, 2011.

- [6] Kai Han, Yunhe Wang, Hanting Chen, Xinghao Chen, Jianyuan Guo, Zhenhua Liu, Yehui Tang, An Xiao, Chunjing Xu, Yixing Xu, et al. A survey on vision transformer. *IEEE transactions on pattern analysis and machine intelligence*, 45(1):87–110, 2022.
- [7] Hila Chefer, Shir Gur, and Lior Wolf. Transformer interpretability beyond attention visualization. In *Proceedings of the IEEE/CVF conference on computer vision and pattern recognition*, pages 782–791, 2021.
- [8] Mattia Rigotti, Christoph Miksovic, Ioana Giurgiu, Thomas Gschwind, and Paolo Scotton. Attention-based interpretability with concept transformers. In *International conference on learning representations*, 2021.
- [9] Bowen Pan, Rameswar Panda, Yifan Jiang, Zhangyang Wang, Rogerio Feris, and Aude Oliva. Interpretability-aware redundancy reduction for vision transformers. *Advances in neural information processing systems*, 34:24898–24911, 2021.
- [10] Chulhee Yun, Srinadh Bhojanapalli, Ankit Singh Rawat, Sashank J Reddi, and Sanjiv Kumar. Are transformers universal approximators of sequence-to-sequence functions? *arXiv preprint arXiv:1912.10077*, 2019.
- [11] Jorge Pérez, Pablo Barceló, and Javier Marinkovic. Attention is turing-complete. *Journal of Machine Learning Research*, 22(75):1–35, 2021.
- [12] Kwangjun Ahn, Xiang Cheng, Hadi Daneshmand, and Suvrit Sra. Transformers learn to implement preconditioned gradient descent for in-context learning. *Advances in Neural Information Processing Systems*, 36:45614–45650, 2023.
- [13] Bingbin Liu, Jordan T Ash, Surbhi Goel, Akshay Krishnamurthy, and Cyril Zhang. Transformers learn shortcuts to automata. *arXiv preprint arXiv:2210.10749*, 2022.
- [14] Haiyan Zhao, Hanjie Chen, Fan Yang, Ninghao Liu, Huiqi Deng, Hengyi Cai, Shuaiqiang Wang, Dawei Yin, and Mengnan Du. Explainability for large language models: A survey. *ACM Transactions on Intelligent Systems and Technology*, 15(2):1–38, 2024.
- [15] Tilman Räuker, Anson Ho, Stephen Casper, and Dylan Hadfield-Menell. Toward transparent ai: A survey on interpreting the inner structures of deep neural networks. In *2023 IEEE conference on secure and trustworthy machine learning (satml)*, pages 464–483. IEEE, 2023.
- [16] Samira Abnar and Willem Zuidema. Quantifying attention flow in transformers. *arXiv preprint arXiv:2005.00928*, 2020.
- [17] Devin Kreuzer, Dominique Beaini, Will Hamilton, Vincent Létourneau, and Prudencio Tossou. Rethinking graph transformers with spectral attention. *Advances in Neural Information Processing Systems*, 34:21618–21629, 2021.
- [18] Jean-Michel Bony. Calcul symbolique et propagation des singularités pour les équations aux dérivées partielles non linéaires. In *Annales scientifiques de l’École normale supérieure*, volume 14, pages 209–246, 1981.
- [19] Hajer Bahouri. *Fourier analysis and nonlinear partial differential equations*. Springer, 2011.
- [20] Raphaël Danchin. Fourier analysis methods for pdes. *Lecture notes*, 14(1):1–91, 2005.
- [21] Lars Hörmander. The nash-moser theorem and paradifferential operators. In *Analysis, et cetera*, pages 429–449. Elsevier, 1990.
- [22] Oluwadamilola Fasina. Quasilinearization with regularizing tensor paraproducts. *arXiv preprint arXiv:2503.12629*, 2025.
- [23] Ronald R Coifman and Matan Gavish. Harmonic analysis of digital data bases. *Wavelets and Multiscale Analysis: Theory and Applications*, pages 161–197, 2011.
- [24] Matan Gavish and Ronald R Coifman. Sampling, denoising and compression of matrices by coherent matrix organization. *Applied and Computational Harmonic Analysis*, 33(3):354–369, 2012.

- [25] Jerrod Isaac Ankenman. *Geometry and analysis of dual networks on questionnaires*. Yale University, 2014.
- [26] Gal Mishne, Ronen Talmon, Ron Meir, Jackie Schiller, Maria Lavzin, Uri Dubin, and Ronald R Coifman. Hierarchical coupled-geometry analysis for neuronal structure and activity pattern discovery. *IEEE Journal of Selected Topics in Signal Processing*, 10(7):1238–1253, 2016.
- [27] Anastasia Georgiou, Arjun Manoj, Pei-Chun Su, Ronald Coifman, Ioannis Kevrekidis, and Somdatta Goswami. From clutter to clarity: Emergent neural operators via questionnaire metrics. 2024.
- [28] David W Sroczynski, Felix P Kemeth, Anastasia S Georgiou, Ronald R Coifman, and Ioannis G Kevrekidis. From disorganized data to emergent dynamic models: Questionnaires to partial differential equations. *PNAS nexus*, page pgaf018, 2025.
- [29] Matan Gavish, Boaz Nadler, and Ronald R Coifman. Multiscale wavelets on trees, graphs and high dimensional data: theory and applications to semi supervised learning. In *ICML*, volume 10, pages 367–74, 2010.
- [30] Yves Meyer. *Ondelettes et opérateurs. I: Ondelettes*, 1990.
- [31] Stephane G Mallat. A theory for multiresolution signal decomposition: the wavelet representation. *IEEE transactions on pattern analysis and machine intelligence*, 11(7):674–693, 1989.
- [32] Ronald R Coifman and M Victor Wickerhauser. Wavelets and adapted waveform analysis. In *Wavelets*, pages 399–423. CRC Press, 2021.
- [33] Anna C Gilbert. Multiresolution homogenization schemes for differential equations and applications. In *Topics In Analysis And Its Applications: Selected Theses*, pages 153–268. World Scientific, 2000.
- [34] William Edward Leeb. *Topics in metric approximation*. 2015.
- [35] Zihang Dai, Zhilin Yang, Yiming Yang, Jaime Carbonell, Quoc V Le, and Ruslan Salakhutdinov. Transformer-xl: Attentive language models beyond a fixed-length context. *arXiv preprint arXiv:1901.02860*, 2019.
- [36] Alexey Dosovitskiy, Lucas Beyer, Alexander Kolesnikov, Dirk Weissenborn, Xiaohua Zhai, Thomas Unterthiner, Mostafa Dehghani, Matthias Minderer, Georg Heigold, Sylvain Gelly, et al. An image is worth 16x16 words: Transformers for image recognition at scale. *arXiv preprint arXiv:2010.11929*, 2020.
- [37] Ronald R Coifman and Stéphane Lafon. Diffusion maps. *Applied and computational harmonic analysis*, 21(1):5–30, 2006.
- [38] Stephen Merity, Caiming Xiong, James Bradbury, and Richard Socher. Pointer sentinel mixture models. *arXiv preprint arXiv:1609.07843*, 2016.
- [39] Alex Krizhevsky. Learning multiple layers of features from tiny images. Technical Report TR-2009, University of Toronto, 2009.

A Proofs

Corollary 2. *If we assume that for a network $T : \{t_i\}_{i=1}^n \rightarrow \hat{v}_m$, $L(v, \hat{v}_m) \rightarrow 0, \forall \hat{v}_m \in \mathcal{X}$, as $||[P^{j+1}P^{j'+1}(f) - P^jP^{j'+1}(f) - P^{j+1}P^{j'}(f) + P^jP^{j'}(f)]|| \rightarrow \infty$ holds, then the softmax activation on a mixed α -Holder attention head can be decomposed into:*

$$\begin{aligned} A(\tilde{f}) &= [P^{j+1}P^{j'+1}(f) - P^jP^{j'+1}(f) - P^{j+1}P^{j'}(f) + P^jP^{j'}(f)] \\ &+ [P^{j+1}P^{j'}(f) - P^jP^{j'}(f)][P^jP^{j'+1}(f) - P^jP^{j'}(f)] + \Delta_{N,N'}(A, f) \end{aligned} \quad (22)$$

where L is a loss function, $\{t_i\}_{i=1}^n$ is a set of tokens input to the model, \hat{v}_m is a prediction from T , v is a ground truth, and \mathcal{X} is a set containing possible predictions of T and the ground truth solution, and $P^jP^{j'}(f)$ is the averaging operator defined in section 3.

Proof. The intuition behind the corollary lies in the assumption: if the loss between the predicted and ground truth tokens decrease as the wavelet coefficients, $||[P^{j+1}P^{j'+1}(f) - P^jP^{j'+1}(f) - P^{j+1}P^{j'}(f) + P^jP^{j'}(f)]||$, of the self-attention matrix, f , tend to infinity, then it follows that the self-attention matrices with large wavelet coefficients helps the network learn.

Thus, if we only consider self-attention matrices, $\{f_i\}_{i=1}^k$, with the property of $||[P^{j+1}P^{j'+1}(f) - P^jP^{j'+1}(f) - P^{j+1}P^{j'}(f) + P^jP^{j'}(f)]|| \rightarrow \infty$. We can show the collection of associated mixed α -Holder functions $\{\tilde{f}_i\}_{i=1}^k$ are invariant to the softmax activation. Let A be the softmax activation function acting on some \tilde{f}_m with the aforementioned property. Then the constants, $A'(P^jP^{j'}(\tilde{f}_m)) = A''(P^jP^{j'}(\tilde{f}_m)) = e^{P^jP^{j'}(\tilde{f}_m)} = e^0 = 1$, since as $||[P^{j+1}P^{j'+1}(\tilde{f}_m) - P^jP^{j'+1}(\tilde{f}_m) - P^{j+1}P^{j'}(\tilde{f}_m) + P^jP^{j'}(\tilde{f}_m)]|| \rightarrow \infty$, $\mu(\tilde{f}_m) \rightarrow 0$, where $\mu(\tilde{f}_m)$ is the average of \tilde{f}_m . As the choice of $\tilde{f}_m \in \{f_i\}_{i=1}^k$ is arbitrary, the result holds for any attention-matrix with the specified property. □

B More experiments

B.1 Top/Bottom Attention Heads

To illustrate how our methodology could be deployed for model pruning, we computed the l_1 entropy of each attention head in both networks with respect to the query-key tensor basis. We collected all network heads in the top 10 percent of l_1 entropies across 6 batches of data and did the same for the bottom 10 percent of l_1 entropies. We then extracted the top 3 and bottom 3 most commonly occurring attention heads in the top and bottom 10 percent of both networks and reported their modes on the right most column. The mode for the attention heads for the top 3 and bottom 3 attention heads appearing in the top and bottom 10 percent of network entropies is 6, meaning they appear in all batches considered for both networks. This suggests, the same attention heads do most of the processing regardless of the data seen, and perhaps more consequentially, the same attention heads do the fewest processing. The latter result implies one could remove attention heads with low l_1 entropy invariant to data from the network, potentially saving computation time.

B.2 Tri-Haar Basis

The structure of the entire network, and not just individual attention heads, can be understood through the lens of the tri-haar basis. We select 100 tri-haar basis vectors with the largest support size, and project each network 3-tensor into the tri-haar basis.

In table 2, we consider 5 batches of network tensor data from the WikiText-103 and CIFAR-10 datasets. The l_1 entropy is computed by summing the expansion coefficients of the largest 100 tri-haar basis vectors. Note there is no correlation between the two columns as each network is processing different batches. Of note, the l_1 entropies for TXL are consistently comparatively

Table 1: Top and Bottom l_1 Entropies of Attention Heads across 6 batches of data

Top 3/Bottom 3 (TXL)	(Layer, Head)	Count
1	(13,3)/(6,0)	6/6
2	(1,0)/(7,5)	6/6
3	(7,7)/(3,5)	6/6
Top 3/Bottom 3 (VIT)	(Layer, Head)	Count
1	(2,5)/(2,4)	6/6
2	(3,6)/(3,10)	6/6
3	(2,10)/(1,11)	6/6

larger than VIT which can be interpreted as the TXL network processing more high frequency content than VIT due to the architectural set-up, but it is most likely related to the data being processed.

Table 2: l_1 entropies of the TXL and VIT networks for 5 batches of WikiText-103 and CIFAR-10 data, respectively

Batch ID	VIT	TXL
1	6.84	1200.20
2	3.30	2473.37
3	2.47	2476.25
4	5.47	1902.98
5	9.77	2188.69

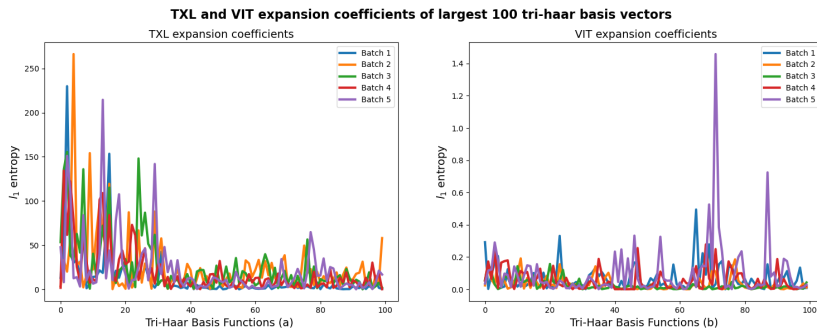


Figure 6: TXL and VIT network entropies with respect to 100 tri-haar basis vectors with largest support size (a) VIT network entropies (b) TXL network entropies

We visualized the expansion coefficients for the top 100 tri-haar basis vectors for the TXL and VIT networks for 5 batches associated with the WikiText-103 and CIFAR-10-10 datasets. The distribution of expansion coefficients is relatively consistent for both networks, with the TXL expansion coefficients being comparatively larger. Both table 2 and figure 6 suggests the proposed methodology is suitable for comparative analysis amongst different networks and datasets.

C Experimental Details

C.1 Experimental results and reproducibility/settings and details/compute resources

TXL/WikiText-103

We trained the transformer-xl (TXL) model TXL on the WikiText-103 dataset. We used a model dimension (i.e. dimension of each token) of 410 with a context length of 256. We set the number of self-attention layers to 16, with each layer containing 8 attention heads. We trained with the adam optimizer with a learning rate of 2.5×10^{-3} . During test time, we randomly select all 128 network attention heads associated with 10 batches (collection of 256 tokens) of data. This model was trained with NVIDIA's A100 GPU.

VIT/CIFAR-10

We trained the vit b16 model VIT on the CIFAR-10 dataset. We use pre-trained ViT B/16 weights and perform 1 epoch of fine-tuning training. We used the adam optimizer with a learning rate of 3×10^{-5} and cross entropy loss. During test time, we randomly select all 144 network attention heads associated with 10 batches (collections of 197 tokens of data) This model was trained with NVIDIA's T4 GPU.

C.2 Open access to data and code

All datasets used are publicly available. The code can be found at <https://github.com/obfasina/OrganizedAttention/>

C.3 Experimental statistical significance

All computational experiments are done to demonstrate potential use cases; no general claims are made about concerning network inference. Thus, we do not consider the statistical significance of our results.